Science Advances

AAAS

advances.sciencemag.org/cgi/content/full/4/1/e1701121/DC1

Supplementary Materials for

The largest deep-ocean silicic volcanic eruption of the past century

Rebecca Carey, S. Adam Soule, Michael Manga, James White, Jocelyn McPhie, Richard Wysoczanski, Martin Jutzeler, Kenichiro Tani, Dana Yoerger, Daniel Fornari, Fabio Caratori-Tontini, Bruce Houghton, Samuel Mitchell, Fumihiko Ikegami, Chris Conway, Arran Murch, Kristen Fauria, Meghan Jones, Ryan Cahalan, Warren McKenzie

Published 10 January 2018, *Sci. Adv.* **4**, e1701121 (2018)
DOI: 10.1126/sciadv.1701121

The PDF file includes:

Other Supplementary Material for this manuscript includes the following:
(available at advances.sciencemag.org/cgi/content/full/4/1/e1701121/DC1)

- movie S1 (.mov format). GP retrieval from the seafloor.

Supplementary Materials

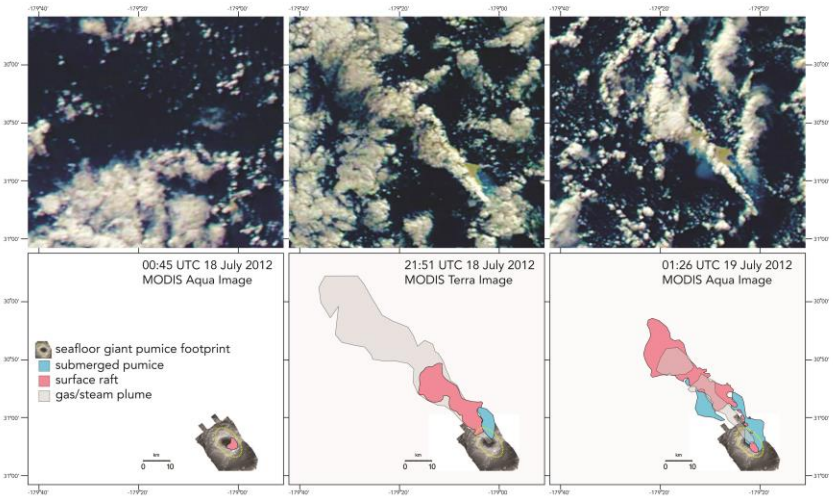

fig. S1. MODIS Terra and Aqua satellite images of the region around Havre volcano collected between 18 and 19 July 2012 (UTC). Images have enhanced colour saturation and the pumice raft can be seen in shades of tan to light brown. The vapor plume originated from a point source identical to the source of the raft, however whether or not particles were present in the plume was not determined. The aqua blue region representing shallow (<200 m below sea level) curtains of submerged pumice adjacent to the raft. The location of the raft is overlain on 2012 multibeam bathymetry of the Havre volcanic edifice in the lower diagrams.

fig. S2. Data collections and tracks

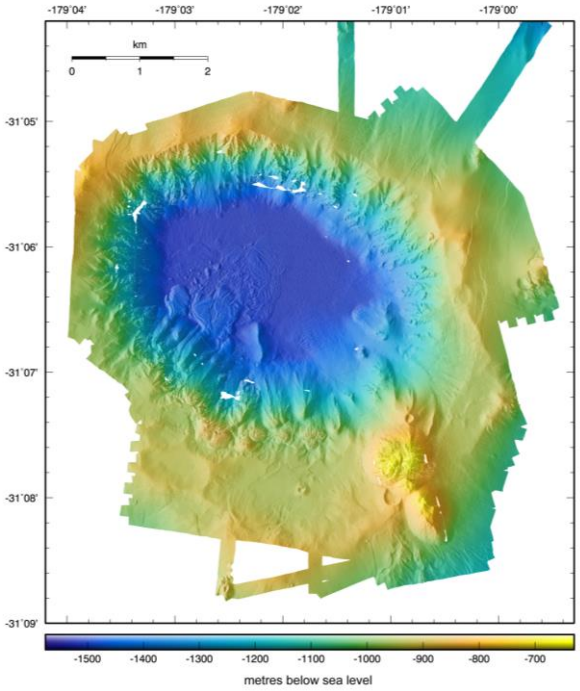

fig. S2.1. AUV high-resolution bathymetry of Havre submarine volcano. Combining the multibeam bathymetric data from 10 AUV *Sentry* deployments yielded a comprehensive, 1 m resolution bathymetric map of the Havre caldera and rim covering over 50 km^2. Data were collected at ~60 m altitude above the seafloor and track spacing was adjusted to account for the steepness of the terrain, but was typically 180 – 200 m (figure S2.2). The sonar returns were corrected for sound-speed velocity and tides, filtered using standard techniques (e.g., removal of outer beams, range gates), and vehicle navigation was corrected for minor offsets using MBSystem. The map shown is illuminated from the west and resolves the newly emplaced lavas and domes, extent of the GP deposit, and areas of mass wasting deposits as well as numerous pre-2012 eruption features at 1-m-scale resolution.

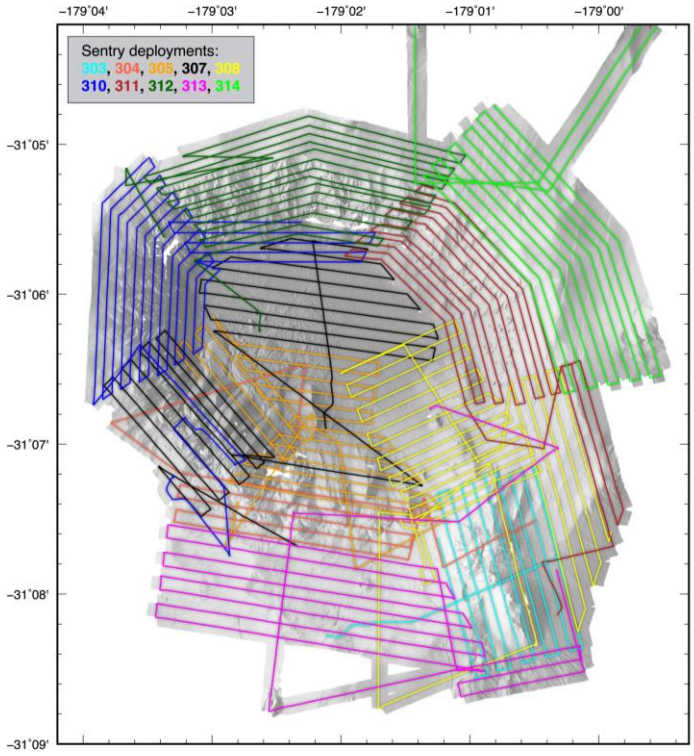

fig. S2.2. Dive tracks for the AUV *Sentry*. The AUV *Sentry* conducted 10 dives covering 465 km of trackline and producing 56.5 km^2 of bathymetry. Each dive trackline is shown in a different colour.

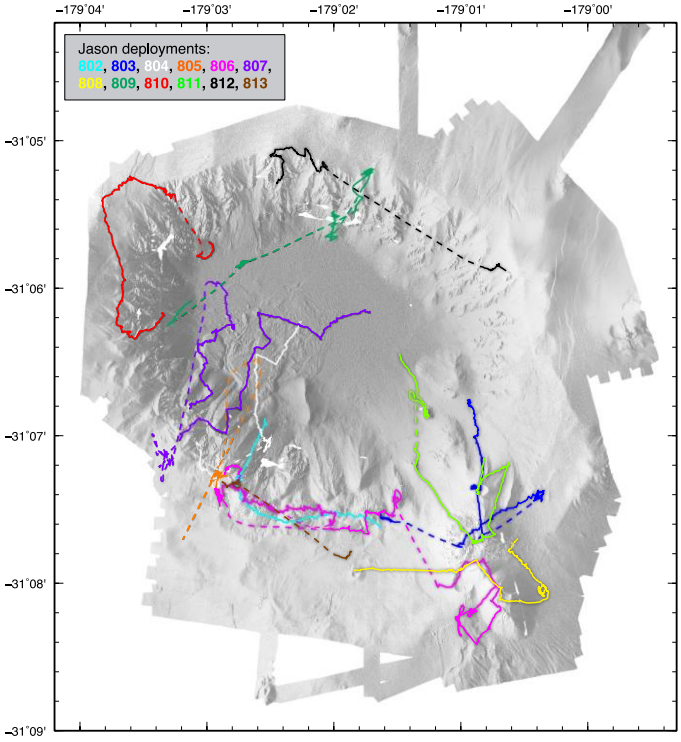

fig. S2.3. ROV track lines. The ROV Jason conducted 12 dives with a total bottom time of 235.8 hours. The locations and dive tracks of each dive are shown in different colors on the map.

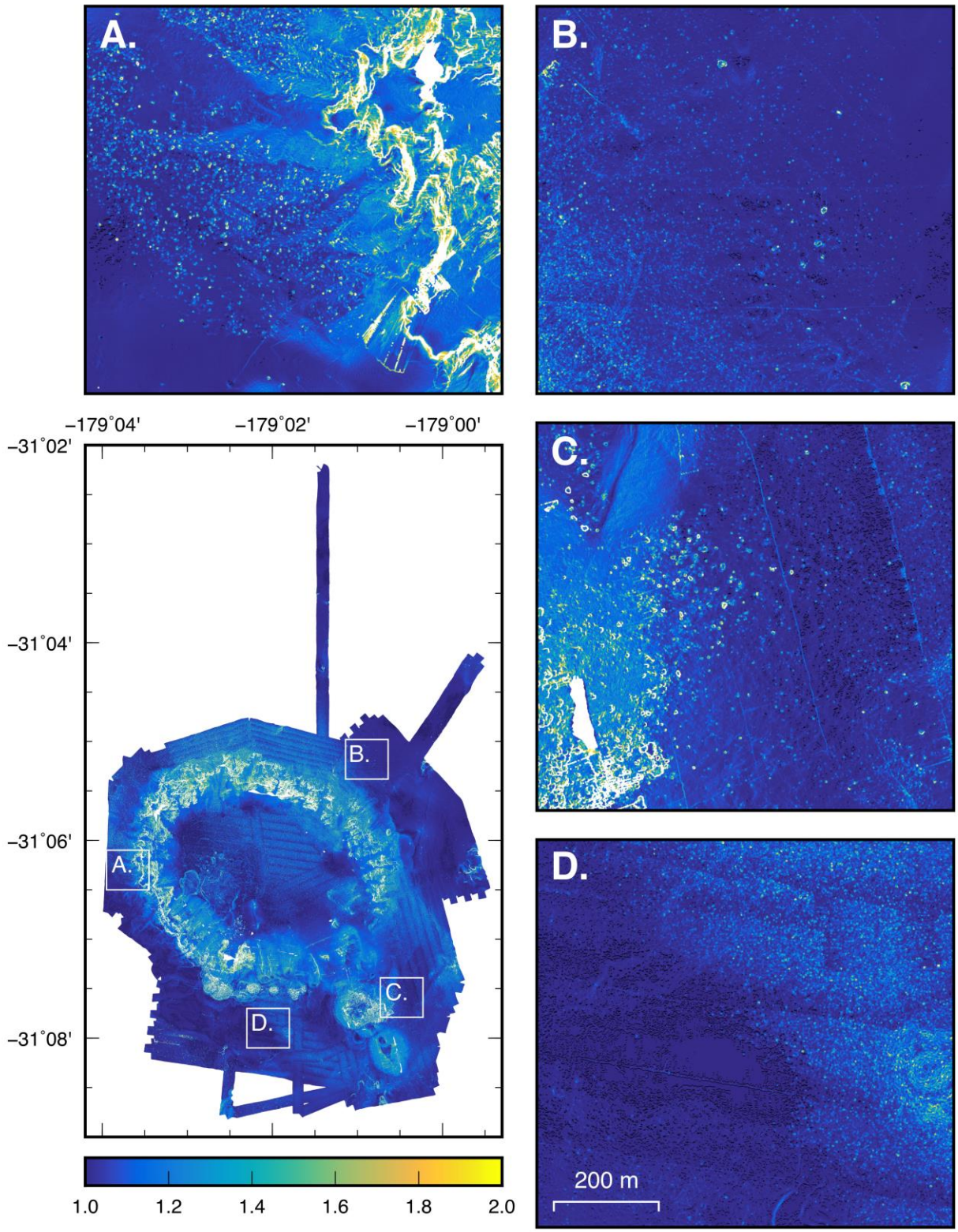
A.
B.
C.
D.
−179°04'
−179°02'
−179°00'
−31°02'
−31°04'
−31°06'
−31°08'
1.0
1.2
1.4
1.6
1.8
2.0
200 m

fig. S3. Detailed views of seafloor roughness. Panels **A**.-**D**. show, at the same scale, detailed views of seafloor roughness derived from the AUV Sentry bathymetric map in units of area of the seafloor relative to a flat seafloor. The location of the detailed maps is shown on the inset at the lower left. Panel A. shows the western boundary of the GP unit indicated by the juxtaposition of smooth seafloor with speckled seafloor resulting from fine-scale relief of the GP. In the upper left, a swath of smooth seafloor probably shows where GP were removed by landslides from the caldera rim and down a chute within the caldera wall. Panel B. shows the northeastern margin of the GP unit, which displays a gradation in roughness over several hundred meters reflecting a more diffuse boundary. Panel C. shows coarse debris shed from dome O-P that overlies the GP and ALB units. Panel D. shows the sharp southwestern margin of the GP unit where dense accumulation of GP gives way to smooth seafloor over tens of metres.

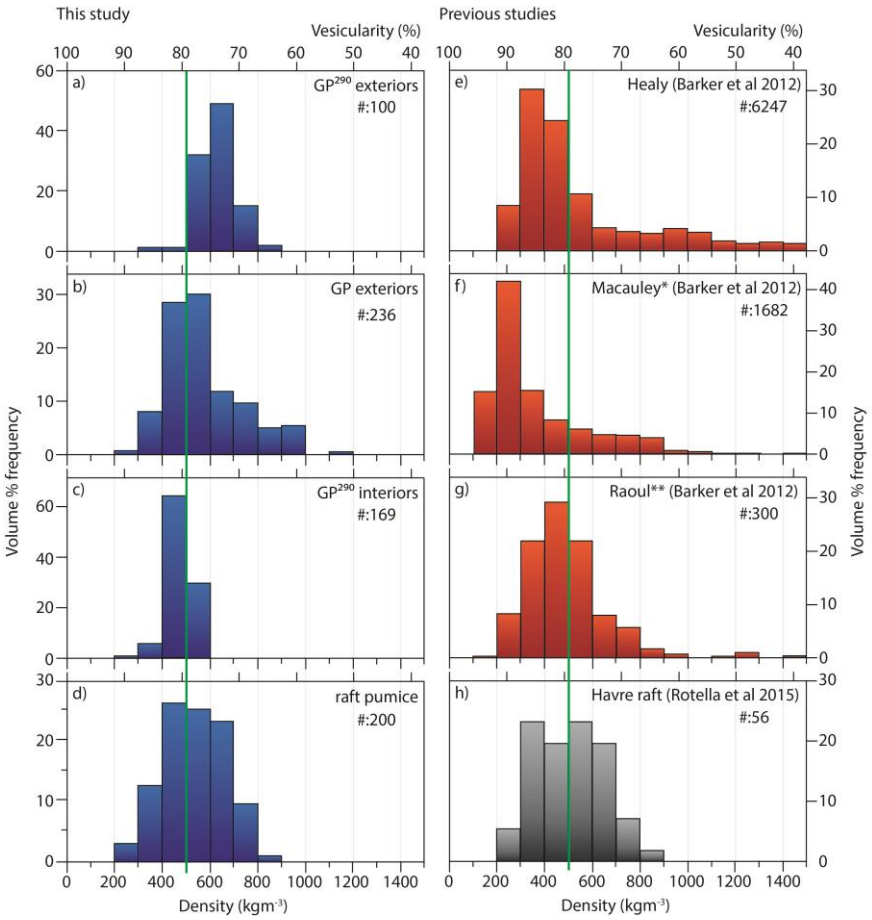

fig. S4. Clast density distributions from Havre and other Kermadec volcanoes. External and internal parts of the GP clast (GP290) retrieved from the seafloor were measured for density (*36*). 16-32 mm fragments were thoroughly washed and dried for 48 hours at < 100°C. Density was derived via Archimedes principle and equivalent bulk vesicularity was calculated using a Dense Rock Equivalent of 2400 kgm^{-3} which is consistent with previous Kermadec pumice studies (*10*, *37*) and calculations from Havre XRF data (table S1a).

Havre pumice density distributions are given here for: GP290 exteriors (a), 10 other GP exteriors sampled (b), GP290 interiors (c), and raft pumice washed ashore in Fiji and collected in 2017 (d). We compare these with distributions from previous Kermadec submarine pumice studies (*10*, *37*) (e - h) noting the similarities in raft pumice sampled directly from the raft soon after the

2012 eruption (H) and those collected over 4 years later (d). Note that c, d and e show data from dredged samples versus our in situ collection of pumice via ROV from a single eruption. GP clasts show a lack of fragments with density < 400 kgm^{-3} in comparison with submarine pyroclasts at Healy, Macauley flanks and Raoul SW.

The green line marks a density of 500 kgm^{-3} which is centered on the modal raft density and GP exteriors for easier comparison with other Kermadec data. Distributions are given as a % fraction of the total number of clasts (#:__).

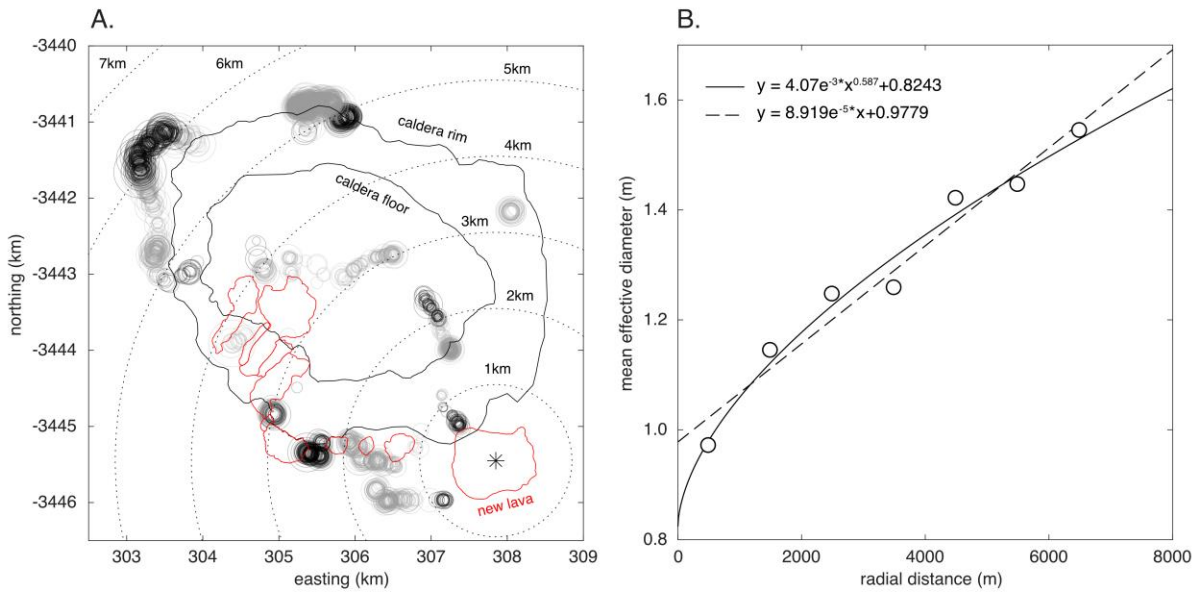

fig. S5. GP size with distance. The sizes of GP clasts were measured from down-looking digital still images collected by ROV Jason. Images contain laser spots spaced at 10cm for scale. The outlines of GP clasts estimated to be greater than 1 m in diameter were manually digitized for ~5000 GP clasts from ~3000 images. We did not digitize pumices for which a significant portion of the clast extended beyond the image frame (typically 3m x 5m) so the results are missing both the smallest and largest GP sizes. The effective diameters of GP clasts were calculated from a circle with equal area to the digitized polygon. The radial transport distance was measured from the center of dome O-P and those GP located NW of the dome O-P center and not on one of the lavas were used to evaluate GP size vs distance. The GP effective diameter within radial transport bins of 1 km were averaged and compared to radial transport distance. There is a clear increase in GP size with distance, consistent with predictions of size-dependent settling due to a presumed positive correlation between GP size and seawater ingestion times *(28)*. These observations, which are limited to the locations ROV Jason, are fit equally well by a linear or exponential relationship between transport distance and size (fig. S2.4B).

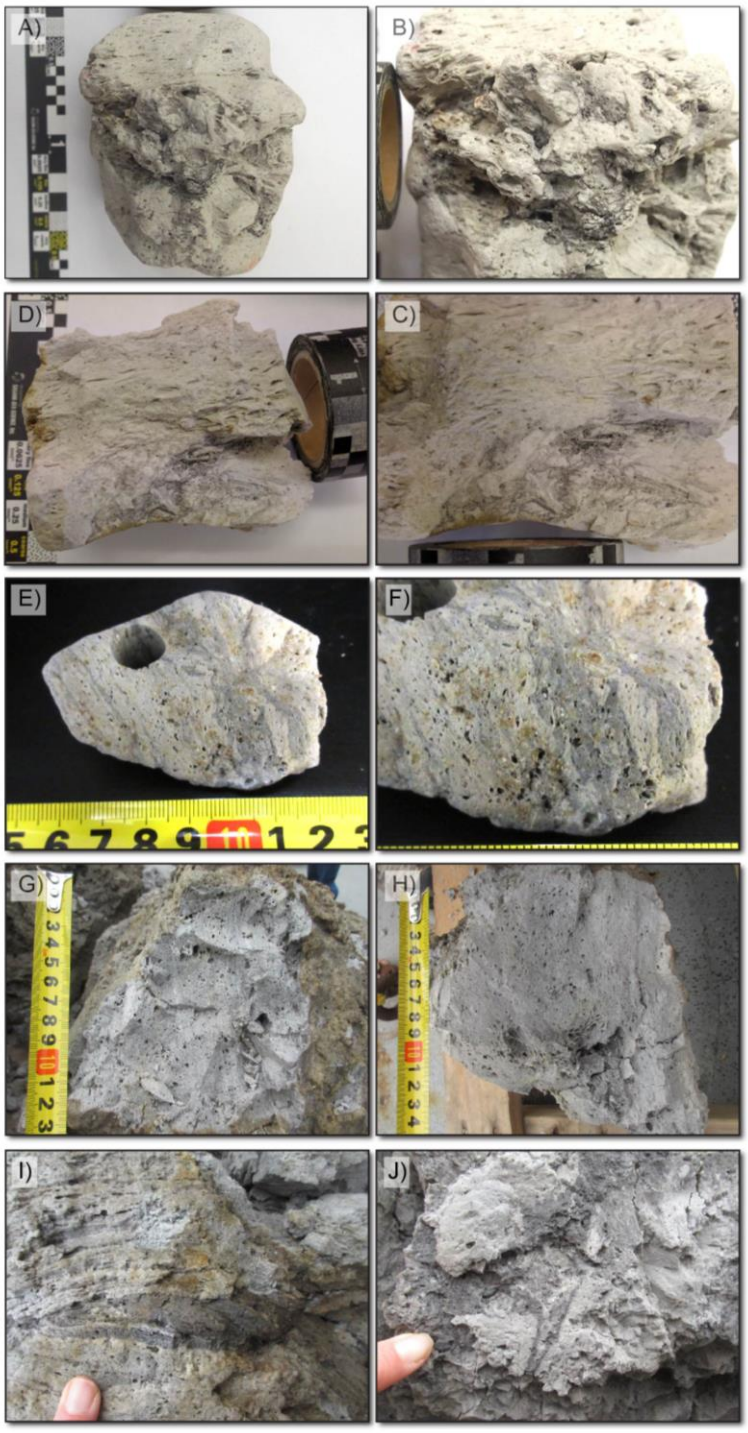

fig. S6. Clast textures from seafloor GP and raft pumice. Photos **A**) to **F**) show banded textures common in pumice sampled from the pumice raft or from New Zealand and Australian

beaches after the July 2012 eruption. Photos **G**) to **J**) show banded textures present in the 1 m x 0.9 m x 0.7 m giant pumice clast retrieved from the seafloor. Fragments from 11 separate giant pumice clasts were sampled with the ROV on the seafloor and reveal similar banding textures. The GP and raft samples are white and vesicular, and commonly have sub-millimeter to millimeter grey irregular sinuous bands. Banding and brecciated zones have not been observed in samples from any other 2012 pumice deposit.

movie S1. GP retrieval from the seafloor. Remotely Operated Vehicle Jason gently extracting a Giant Pumice clast from a field of giant pumice on the seafloor at 900 mbsl. The width of the ROV Jason tray is 1.5 m. The dimensions of this clast are 1 m x 0.9 m x 0.7 m. This sample has an average density of 550 kgm^{-3} and estimated to weigh ~350 kg.

table S1A. X-ray fluorescence geochemical data of 2012 products. Oxide abundances are given in wt. % and normalized to volatile-free totals of 100%. Original LOI values and analytical totals are given. LOI is weight loss on ignition after sample powders were placed in a furnace at 1000°C for 4 hours.

Unit	Sample	SiO2	TiO2	Al2O3	Fe2O3	MnO	MgO	CaO	Na2O	K2O	P2O5	LOI	Total Orig.
A	HVR0170	70.66	0.50	14.41	3.98	0.13	0.82	2.89	5.07	1.42	0.10	1.62	100.81
B	no data												
C	HVR0147	70.89	0.49	14.43	3.79	0.13	0.77	2.85	5.15	1.40	0.10	1.53	100.86
D	HVR0151	70.95	0.49	14.37	3.80	0.13	0.76	2.86	5.05	1.48	0.10	1.31	100.74
E	HVR0150	70.67	0.49	14.28	3.94	0.13	0.79	2.88	5.23	1.48	0.10	1.48	98.67
F	HVR0083	70.92	0.49	14.35	3.81	0.13	0.81	2.85	5.15	1.39	0.10	1.48	100.60
G	HVR0288	71.72	0.47	14.18	3.40	0.12	0.71	2.68	5.22	1.42	0.09	0.43	99.71
H	HVR0086	71.95	0.47	13.99	3.44	0.12	0.66	2.53	4.99	1.77	0.08	1.65	100.23
I	HVR0090	71.95	0.46	13.98	3.45	0.12	0.66	2.56	5.13	1.60	0.08	1.42	100.34
K	HVR0093	71.97	0.46	13.99	3.45	0.12	0.65	2.55	5.21	1.51	0.08	1.22	100.01
L	HVR0099	71.86	0.45	14.02	3.41	0.12	0.64	2.58	5.22	1.62	0.08	1.79	98.57
M	HVR0026	72.01	0.46	13.91	3.42	0.12	0.65	2.53	5.19	1.64	0.08	1.32	98.96
N	HVR0021	71.89	0.46	13.98	3.51	0.12	0.66	2.57	5.25	1.47	0.08	1.64	99.53
O	HVR0010	72.20	0.46	14.10	3.22	0.11	0.71	2.56	5.14	1.42	0.08	0.59	100.61
P	HVR0013	72.21	0.46	14.13	3.28	0.08	0.69	2.55	5.14	1.37	0.08	0.41	100.37
Giant Pumice	HVR0290	71.92	0.47	14.01	3.38	0.12	0.67	2.58	5.14	1.62	0.08	1.27	99.71

table S1B. X-ray fluorescence geochemical precision and accuracy data. Pumice and lava samples were prepared for whole-rock geochemical analysis by cutting away altered surfaces and crushing material to obtain fresh ~1x1 cm pieces, which were washed in running hot water (~50°C) for 7–14 days to leach seawater. Once leached, pieces were broken in an iron mortar into 2–5 mm chips that were then washed in an ultrasonic bath using deionised water and acetone. The cleaned chips were dried in an oven at 110°C for >12 hours and then powdered. Before the major element analysis, 0.4 g of powder was weighed on a Metler Toledo dual balance system and ignited at 1025°C for 4 hours in an electric muffle furnace to determine loss-on-ignition (LOI). After the LOI determination, glass beads containing lithium tetraborate flux (10 to 1 dilution of sample) were prepared. The glass beads were analyzed by X-ray fluorescence (XRF) analysis (Rigaku RIX1000) at the National Museum of Nature and Science for major elements. Values for analytical precision and accuracy, as estimated from repeated analysis of well-established reference standard JB-1, are provided in the table S1b.

	wt% SiO2	TiO2	Al2O3	Fe2O3	MnO	MgO	CaO	Na2O	K2O	P2O5
JB-1 average	52.7	1.3	14.4	8.9	0.2	7.9	9.3	2.8	1.5	0.3
2 s.d.	0.05	0.01	0.02	0.01	0.00	0.01	0.01	0.02	0.00	0.00
JB-1 GeoRem	52.4	1.3	14.5	9.0	0.2	7.7	9.3	2.8	1.4	0.3
% offset	0.55	0.53	-0.70	-0.75	-1.96	2.48	0.68	-0.47	1.40	1.96

table S2. Table of Havre lava volumes. Table of lavas and volume calculations. Volume described in Methods *(23)*. The volumes of lavas F to P are minima as the fragmental deposits on surrounding slopes and mass wasting deposits are not included in the calculations. Lava J is an older pre-2012 eruption product. A lava density of 2350 kgm^{-3} was used given the low porosity of the samples.

Unit/deposit	Volume $x10^6$ m^3	Time-averaged eruption rate (m^3s^{-1})
Lava A	8.9	
Lava B	2.8	
Lava C	34	
Lava D-E	8.2	
Lava F	26	
Lava G	0.4	
Lava H-I	10.6	1.4
Lava K	2.3	0.3
Lava L	1.7	0.22
Lava M-N	5.9	0.8
Lava O-P	109.9	14.1
Giant Pumice (proximal)	100	
Giant Pumice (raft)	1,200	15,504
Ash-Lapilli-Block	5	
Ash-Lapilli	63	

table S3. Phenocryst assemblages and microlite populations of the GP and raft pumice from petrographic analysis. Raft samples analysed were those collected by boat and those washed ashore in Fiji and Australia. Exteriors and interior fragments were analysed from GP290.

Giant pumice:			Raft pumice:		
Phenocryst phases	% Phenocryst abundance	Microlites identified	Phenocryst phases	% Phenocryst abundance	Microlites identified
Plagioclase	3 - 5	Plagioclase	Plagioclase	< 3	Plagioclase
Orthopyroxene	1 - 2	Pyroxene	Orthopyroxene	1	Pyroxene
Quartz	< 1	Oxide	Fe-Ti Oxide	1	Oxide
Fe-Ti Oxide	< 1		Quartz	< 1	
Clinopyroxene	<< 1		Clinopyroxene	<< 1	
Total	4 - 8			2 - 5	